

# Registration Strategies and Similarity Measures for Three-Dimensional Ultrasound Mosaicing

Christian Wachinger Dipl.-Inf. <sup>a,\*</sup> and Wolfgang Wein Dr. <sup>b</sup>  
Nassir Navab Prof. Dr. <sup>a</sup>

<sup>a</sup>*Computer Aided Medical Procedures, TU München, Germany*

<sup>b</sup>*Siemens Corporate Research, Princeton, NJ, USA*

---

## Abstract

**Rationale and Objectives:** The creation of 2D ultrasound mosaics is becoming a common clinical practice with a high clinical value. The next step coming along with the increasing availability of 2D array transducers is the creation of 3D mosaics. The correct alignment of multiple ultrasound images is, however, a complex task. In the literature of ultrasound registration, the alignment of two images was often addressed; however, not the alignment of multiple images. Therefore, we propose registration strategies for multiple image alignment and ultrasound specific similarity measures, which are able to cope with problems arising by aligning ultrasound images.

**Materials and Methods:** In this article, we investigate the following strategies for multiple image alignment: pairwise registration with a successive Lie group normalization and *simultaneous registration*, which urges the usage of *multivariate similarity measures*. We propose alternative multivariate extensions for similarity measures based on a maximum likelihood framework. Moreover, we take the inherent contamination of ultrasound images by speckle patterns into consideration by using alternative noise models based on multiplicative Rayleigh distributed noise. This leads us to ultrasound specific similarity measures.

**Results:** We compare the performances of pairwise and simultaneous registration approaches for the mosaicing scenario. Bivariate similarity measures are highly overlap dependent, so that they rather favor the total overlap of the images than their correct alignment. Using ultrasound specific bivariate measures leads to better results, however, a local optimum at the total overlap remains. In contrast, the derived multivariate similarity measures have a clear and single optimum at the correct alignment of the volumes.

**Conclusion:** The experiments indicate that standard, pairwise registration techniques have problems by aligning multiple ultrasound images with partial overlap. We demonstrate that the usage of an ultrasound specific similarity measure leads to better results for pairwise registration. The highest robustness, however, can be achieved by using simultaneous registration with the developed multivariate similarity measures.

*Key words:* 3D registration, 3D ultrasound, simultaneous registration, mosaicing, multivariate similarity measures, ultrasound specific similarity measures

---

\* Corresponding author. Phone: +49 (89) 289 17071, Fax: +49 (89) 289 17059  
*Email address:* wachinge@cs.tum.edu (Christian Wachinger Dipl.-Inf.).  
*URL:* <http://campar.in.tum.de/Main/ChristianWachinger>  
(Christian Wachinger Dipl.-Inf.).

<sup>1</sup> This research was partially funded by an academic grant from Siemens Medical Solutions, Germany.

## 1 Introduction

At the moment, a paradigm shift takes place in ultrasound (US) imaging, moving from 2D to 3D image acquisition. The next generation of 2D array US transducers with CMUT<sup>2</sup> technology could accelerate this shift by offering superior and efficient volumetric imaging at a lower cost. From a current perspective, the only drawbacks that remain are the limited field-of-view (FOV) of the acquired images and the reflectance of the beam from structures with high acoustic impedance causing occlusion. The idea of mosaicing is to address these issues by combining the information of several images taken from different poses. The focus can rest on quality improvement by imaging the same scene from different directions, or the extension of the FOV by stitching together consecutively taken images. Whatever we are interested in, the first step is to calculate the correct global alignment for which we propose solutions in this report.

The rigid intensity-based registration that we use for the alignment is not trivial to compute because of the limited amount of overlap between the images. This limited overlap puts a special interest on the overlap invariance of the similarity measures, since the perfect alignment does not correspond to a maximal overlap. An additional difficulty lies in the interface enhancing nature of ultrasound images, making acquisitions of the same object but from varying viewing angles not necessarily look the same. In the following we will focus on intensity-based registration, which is mainly used for aligning ultrasound images, but there are also groups working on feature-based approaches [1].

### 1.1 *Clinical value of ultrasound mosaicing*

The usage of ultrasound mosaicing provides the sonographers not just with a compounded volume of higher quality; recent studies also state a couple of other clinical advantages that come along with the extended FOV. First, the spatial relationship among structures that are too large for a single volume is easier to understand [2]. Second, sonographers have the flexibility to visualize anatomical structures from a variety of different angles [3, 4]. Third, size and distance measurements of large organs are possible [2, 5]. Fourth, individual structures within a broader context can be identified by having an image of the whole examination area [6]. And last, because of the increased features in the compounded view, specialists that are used to other modalities than ultrasound can better understand the spatial relationships of anatomical structures [7]; helping to bridge the gap between the modalities and making it easier to convey sonographic findings to other experts.

But it is not just the improvement of already existing workflows, the creation of

---

<sup>2</sup> Capacitive Micromachined Ultrasound Transducer

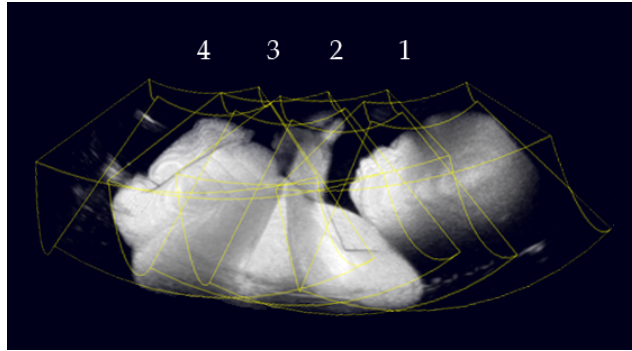


Fig. 1. Volume rendering of compounded baby phantom.

high quality mosaics may also create new medical applications for ultrasound that do not yet exist at all or are reserved for other modalities. Finally, three-dimensional mosaicing could be the application helping 3D imaging to gain widespread access in the clinical practice, which it has not yet [8], although there are studies giving evidence that 3D imaging is superior to 2D imaging [9]. An example mosaic consisting of 4 acquisitions of a baby phantom is shown in Figure 1.

## 1.2 Problems statement

In the literature of ultrasound mosaicing, the global alignment of multiple images is deduced from a sequence of pairwise ones. Gee *et al.* [10] reduce the 3D-3D registration problem to a 2D-2D one by registering the dividing planes to each other. Poon *et al.* [11] use a block-based rigid and block-based warping approach for the registration. The disadvantages that come along with the usage of pairwise registrations for ultrasound mosaicing are twofold. First, by stitching together pairwise aligned images, registration errors can be accumulated leading to a non-consistent global alignment. Second, during the pairwise registrations only a fraction of the available information is taken into account making it prone to misregistrations. The registration is further complicated by the viewing angle dependent US images and the high demands on the overlap invariance by mosaicing.

Moreover, sonography suffers from artifacts caused by coherent wave interference known as speckle. Speckle limits low resolution image contrast and may even obscure true structures in high contrast regions. Since speckle is a spatially correlated noise patterns, it is a common strategy to use it in ultrasound motion estimation, particularly in cardiac imaging [12]. The correlation between the speckle patterns, however, vanishes for images having larger displacements and being acquired from different viewing-angles. Therefore, a usual pre-processing step for ultrasound registration is to reduce the speckle noise by *e.g.* low-pass filtering with a Gaussian [10,13] or coherence-enhancing diffusion filtering [14]. Frequently used similarity measures implicitly assume a Gaussian distributed noise, although it was shown that for ultrasound images degraded by speckle patterns, a Rayleigh dis-

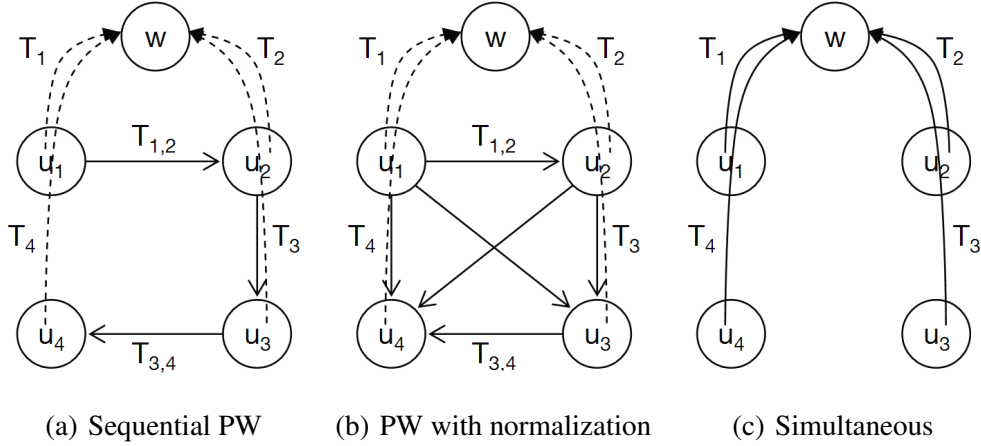


Fig. 2. Registration graphs illustrating different strategies. Solid lines indicating calculated transformations and dashed lines deduced ones. For clarity, not all edges are labeled.

tributed noise is more appropriate [15]. We will use ultrasound specific likelihood terms to deduce bivariate and multivariate similarity measures to make them work in our registration framework, used for 3D ultrasound mosaicing.

## 2 Mosaicing Strategies

In this section, we present registration strategies that directly address the problems that arise during the mosaic creation as mentioned in section 1.2. We denote the  $n$  ultrasound images by  $\mathcal{U} = \{u_1, \dots, u_n\}$  with the global transformations  $\mathcal{T} = \{T_1, \dots, T_n\}$ , and the pairwise transformation  $T_{i,j}$  between each overlapping image pair  $u_i$  and  $u_j$ . The strategies are schematically shown in Figure 2, with the images as nodes and the transformations as edges. To illustrate the global transformations that we are finally interested in, we augment the graph with a world node  $w$ . In Figure 2(a) the standard strategy, which is based on a minimal number of pairwise registrations, is depicted. For the illustrated scenario with 4 images, 3 pairwise transformations have to be calculated to deduce the global alignment. We register neighboring pairs since they share the largest overlap.

### 2.1 Pairwise registration with Lie normalization

The first strategy we propose is based on pairwise registrations and uses a consecutive normalization to reduce the accumulated error. To this end, all pairwise registrations of overlapping pairs are calculated. The over-determined equation system we end up with to deduce the global transformations, makes a normalization necessary. Supposing all images to be overlapping, this results in a complete graph, see Figure 2(b).

Assuming that we would have all correct global transformations  $T_i$ , we could express the pairwise error transformation  $\tau_{i,j}$  as

$$\tau_{i,j} = T_i^{-1} \cdot T_j \cdot T_{i,j}. \quad (1)$$

In practice, the opposite holds since we know the pairwise registrations  $T_{i,j}$  and use them to estimate the global transformations  $T_i$ . The best estimation of the global alignment is reached when the overall error is minimized. The minimization is not trivial because rigid transformations do not belong to a vector space but rather lie on a non-linear manifold forming a Lie group [16]. We use the Lie group based normalization framework, as it was proposed by Vercauteren *et al.* [17] for the alignment of 2D optical images, to align 3D ultrasound images. An error function  $\mu_\tau$  is introduced to assign each error transformation  $\tau_{i,j}$  an error value serving as score for the optimization. Assuming  $\tau_{i,j}$  being a sample of the random error  $\varepsilon$  with Fréchet matrix mean identity and covariance matrix  $\Sigma_{\tau\tau}$ , the Mahalanobis distance that we use as error function is

$$\mu_\tau^2(\tau_{i,j}) = \log_{\text{Id}}(\tau_{i,j})^T \cdot \Sigma_{\tau\tau}^{-1} \cdot \log_{\text{Id}}(\tau_{i,j}). \quad (2)$$

- 
- (1) Start with initial global transformations  $\mathcal{T} = \{T_1, \dots, T_n\}$
  - (2) **Do**
    - 2.1 Deduce initial pairwise transformations  $T_{i,j}$  from  $\mathcal{T}$  using  $T_{i,j} = T_j^{-1} \cdot T_i$
    - 2.2 Compute all pairwise registrations  $T_{i,j}$  with intensity-based rigid registration
    - 2.3 Estimate new  $\mathcal{T}$  from calculated  $T_{i,j}$  with Lie group normalization in Equ. (3)
  - (3) **While** ( $\tau_t > \delta$ )
  - (4) **Return**  $\mathcal{T}$
- 

Table 1  
Algorithm for pairwise registration with Lie group normalization.

The global pose estimation is expressed by the following least-squares criterion

$$[\hat{T}_1, \dots, \hat{T}_n] = \arg \min_{[T_1, \dots, T_n]} \frac{1}{2} \sum_{(i,j)} \omega_{i,j} \cdot \mu_\tau^2(\tau_{i,j}). \quad (3)$$

with the quality weights  $\omega_{i,j}$ . These weights model the quality of each pairwise registration. Since we are interested in an automated registration we use the amount of overlap as an indicator of the registration quality. The final algorithm using the Lie group normalization is stated in Table 1. The registration is accepted if the total error  $\tau_t = \sum_{(i,j)} \omega_{i,j} \cdot \mu_\tau^2(\tau_{i,j})$  is below a scenario dependent threshold  $\delta$ . An alternative for using an acceptance criterion based on the absolute error  $\tau_t$  would be to calculate the relative error between two iterations  $\tau_t^{\text{iter}} - \tau_t^{\text{iter}-1}$ .

## 2.2 Simultaneous Registration

The second strategy is based on simultaneous registration which is an active field of research and has so far mainly been used for population studies [18] in medical imaging. In computer vision, the simultaneous registration was already used earlier for aligning multiple surfaces [19]. The principle of simultaneous registration is to consider all available images at the same time during the registration process. Since we are directly optimizing the global transformations, the deduction of the global alignment from local alignments becomes superfluous, see Figure 2(c). To make this possible, the registration framework has to be extended to deal with multivariate similarity measures and the simultaneous optimization of  $n \cdot 6$  parameters. Up to now, only a limited number of multivariate extensions for popular measures have been proposed, which we discuss together with our own extensions in section 3.

The reason for choosing a simultaneous registration approach is twofold, like the problems occurring during registration. First, the accumulated registration error that was treated in a separated normalization step by the above mentioned registration approach, is now handled intrinsically during the registration. Second, the multivariate similarity measures create more robust cost functions for the optimizer to run on because each image is put into its global context trying to get the maximal information out of the depicted structures.

- 
- (1) **For** number of cycles
    - 1.1 **For** each  $i$  in  $\{1, \dots, n\}$ 
      - 1.1.1 Simultaneously register image  $u_i$  to  $\{u_1, \dots, u_{i-1}, u_{i+1}, \dots, u_n\}$  for  $k$  optimization steps, changing matrix  $T_i$
    - 1.2 **END**
  - (2) **END**
  - (3) Return  $\mathcal{T}$
- 

Table 2

Algorithm for semi-simultaneous registration.

For our mosaicing framework we use two variants of the simultaneous approach that we refer to as *full-simultaneous* and *semi-simultaneous* registration, both using multivariate similarity measures but differing in their optimization strategy. While for the full-simultaneous registration the optimization is performed in the  $n \cdot 6$  dimensional parameter space, the semi-simultaneous registration focuses on the optimization of the 6 pose parameters of one image at a time. During one cycle each image is registered for a limited number of registration steps  $k$ . Several of these cycles yield a stepwise simultaneous convergence to the best global alignment. The algorithm for semi-simultaneous registration is listed in Table 2.

The reason for working with two versions lies in the increased computational complexity of simultaneous methods, which is a logical consequence of the higher di-

dimensional parameter space and multivariate similarity metrics. The semi-simultaneous approach has lower complexity because of the reduced parameter space and because we can limit the evaluation of the similarity measure to the grid of the currently optimized image. A complete drift of the scene is avoided by normalizing the transformations so that one of them be the identity.

### 3 Multivariate Similarity Measures

Multivariate similarity measures have not yet been used for the registration of multiple ultrasound images in spite of their already mentioned advantages. In this section, we focus our analysis on four popular measures, whose applications are not limited to ultrasound registration: sum of squared differences (SSD), normalized cross-correlation (NCC), mutual information (MI), and correlation-ratio (CR). In section 4, we focus on ultrasound specific similarity measures. A maximum-likelihood estimation (MLE) framework is commonly used to mathematically model the registration process. For the bivariate case the imaging process is described by  $u(x) = f(v(T(x))) + \varepsilon$ , with the images  $u$  and  $v$ , the transformation  $T$ , the intensity mapping  $f$ , and the Gaussian distributed random variable  $\varepsilon$  modeling the noise. The log-likelihood function is

$$\log \mathcal{L}(T, \varepsilon, f) = \log P(u|v, T, \varepsilon, f) = \log P(\varepsilon = u(x) - f(v(T(x)))) \quad (4)$$

with  $P$  the probability density function (PDF). In the work of Viola [20] and Roche *et al.* [21] the deduction of the four measures based on this equation is shown by varying the assumptions for the intensity mapping. We are extending this approach to multiple images under the assumption of conditional independent images. The extended MLE denoting the transformed images  $u_i^\downarrow = u_i(T_i(\cdot))$  is

$$\log \mathcal{L}(\mathcal{T}, \vec{\varepsilon}, \vec{f}) = \log P(u_1^\downarrow | u_2^\downarrow, \dots, u_n^\downarrow, \vec{\varepsilon}, \vec{f}) \quad (5)$$

$$= \log P(\varepsilon_2 = u_1^\downarrow - f_2(u_2^\downarrow), \dots, \varepsilon_n = u_1^\downarrow - f_n(u_n^\downarrow)) \quad (6)$$

$$= \sum_{i=2}^n \log P(\varepsilon_i = u_1^\downarrow - f_i(u_i^\downarrow)) \quad (7)$$

with intensity mappings  $\vec{f} = (f_2, \dots, f_n)$  and Gaussian noises  $\vec{\varepsilon} = (\varepsilon_2, \dots, \varepsilon_n)$ . Each summand corresponds to the bivariate formula in equation (4) and the deduction of the four similarity measures can therefore be done analogously as in [20, 21]. This shows that we directly obtain multivariate extensions of that form by summing up the bivariate measures. In this type of extension we pick one reference image, in the formulae above  $u_1$ , which suits very well for the semi-simultaneous registration approach. Setting up a similarity matrix  $M$  with the entries  $M_{i,j} = SM(u_i, u_j)$ , this corresponds to summing up its first row. An adaptation of this approach to the full-simultaneous registration is obtained by summing up the whole similarity matrix,

	Pairwise	Semi-Simultaneous	Full-Simultaneous	Voxel-Wise
SSD	$\mathbb{E}[(u - v^\downarrow)^2]$	$\sum_{i=2}^n \omega_{1,i} \mathbb{E}[(u_1 - u_i^\downarrow)^2]$	$\sum_{i<j} \omega_{i,j} \mathbb{E}[(u_i^\downarrow - u_j^\downarrow)^2]$	$\sum_{x_k \in \Omega} \omega_k \mathbb{E}_i[(\mu_k - u_i^\downarrow(x_k))^2]$
NCC	$\mathbb{E}[\tilde{u} \cdot \tilde{v}^\downarrow]$	$\sum_{i=2}^n \omega_{1,i} \mathbb{E}[\tilde{u}_1 \cdot \tilde{u}_i^\downarrow]$	$\sum_{i<j} \omega_{i,j} \mathbb{E}[\tilde{u}_i^\downarrow \cdot \tilde{u}_j^\downarrow]$	$\sum_{x_k \in \Omega} \omega_k \mathbb{E}[\tilde{u}_1^\downarrow \cdot \tilde{u}_2^\downarrow \cdots \tilde{u}_n^\downarrow]$
CR	$\frac{\text{Var}[\mathbb{E}(u v^\downarrow)]}{\text{Var}(u)}$	$\sum_{i=2}^n \omega_{1,i} \frac{\text{Var}[\mathbb{E}(u_1 u_i^\downarrow)]}{\text{Var}(u_1)}$	$\sum_{i \neq j} \omega_{i,j} \frac{\text{Var}[\mathbb{E}(u_i^\downarrow u_j^\downarrow)]}{\text{Var}(u_i^\downarrow)}$	-
MI	$\text{MI}(u, v^\downarrow)$	$\sum_{i=2}^n \omega_{1,i} \text{MI}(u_1, u_i^\downarrow)$	$\sum_{i<j} \omega_{i,j} \text{MI}(u_i^\downarrow, u_j^\downarrow)$	$\sum_{x_k \in \Omega} \omega_k H(P^k)$

Table 3

Summary of bi- and multivariate similarity measures in shortened notation.

which can often be limited to the upper triangular part because of the symmetry of the measures. Additionally, the pairs are weighted by an overlap dependent factor  $\omega_{i,j}$  emphasizing pairs with high overlap. The final similarity measures are shown in Table 3.

A second type of extension, the *voxel-wise* one, that we are using is based on the idea of congealing [18] and puts the focus on a voxel location at a time. In the MLE framework, it is integrated by estimating PDFs for each voxel under the assumption of independent but not identical distributed coordinate samples

$$\log \mathcal{L}(T) = \log P(u_1^\downarrow, u_2^\downarrow, \dots, u_n^\downarrow) \quad (8)$$

$$= \frac{1}{|\Omega|} \log \prod_{x_k \in \Omega} P^k(u_1^\downarrow(x_k), \dots, u_n^\downarrow(x_k)) \quad (9)$$

$$\approx \frac{1}{|\Omega|} \sum_{x_k \in \Omega} \log \prod_{i=1}^n P^k(u_i^\downarrow(x_k)) \quad (10)$$

with the grid  $\Omega$ . By further assuming a Gaussian distribution of values at each location with mean  $\mu_k$  and variance  $\sigma_k^2$  the log-likelihood function is

$$\log \mathcal{L}(T) = \frac{1}{|\Omega|} \sum_{x_k \in \Omega} \sum_{i=1}^n \log \left( \frac{1}{\sqrt{2\pi\sigma}} e^{-\frac{1}{2} \frac{(u_i^\downarrow(x_k) - \mu_k)^2}{\sigma_k^2}} \right) \quad (11)$$

$$\approx -\frac{1}{|\Omega|} \sum_{x_k \in \Omega} \frac{1}{\sigma_k^2} \sum_{i=1}^n (u_i^\downarrow(x_k) - \mu_k)^2. \quad (12)$$

We consider this criterion as a voxel-wise extension of SSD because similar assumptions as for its pairwise deduction in [20] were used. When not taking the assumption of a Gaussian distribution, equation (10) can be further developed like it was done for the congealing by Zollei *et al.* [18]

$$\log \mathcal{L}(T) = \frac{1}{N} \sum_{x_k \in \Omega} \sum_{i=1}^n \log P^k(u_i^\downarrow(x_k)) \quad (13)$$

$$\approx \sum_{x_k \in \Omega} H(P^k) \quad (14)$$

with the sample entropy  $H$ . We added the congealing criterion [18] as an extension of MI to Table 3, because they are both based on the estimation of the entropy  $H$ , although they have different properties. We also use a voxel-wise criterion for NCC that, in our opinion, captures the basic idea of it by multiplying the values at each voxel location of the normalized images  $\tilde{u}_i$ . This is obviously not a rigorous deduction, but rather based on analogies. For all, we added the weighting factor  $\omega_k$  emphasizing locations with a higher number of overlapping images. The usual extensions based on higher-dimensional PDFs are not applicable to mosaicing because they are not flexible enough to allow for varying numbers of overlapping images.

#### 4 Ultrasound specific similarity measures

So far, only the standard similarity measures SSD, NCC, CR, and MI were used for 3D mosaicing, which are not specifically designed for US images. Like already mentioned in the last section, these four measures can be derived from a maximum-likelihood estimation (MLE) assuming a Gaussian distributed noise. For ultrasound images this is not the best choice, because they contain speckle patterns changing the characteristics of the image, and leading to a better approximation by a Rayleigh distributed noise [15]. Based on this noise assumption Strintzis, Kokkindis [22] and Cohen, Dinstein [23] developed likelihood terms for US motion estimation denoted by  $SK_1$ ,  $SK_2$  and  $CD_1$ ,  $CD_2$ , respectively.

We will use these ultrasound specific likelihood terms to deduce bivariate similarity measures and, in a second step, extend them to multivariate measures to make them work in our registration framework, used for 3D ultrasound mosaicing. The good results of Boukerroui et al. [24] and Revell et al. [25], who used a bivariate extension of  $CD_2$ , further encouraged our intentions for its investigation.

##### *SK<sub>1</sub>: Multiplicative Rayleigh noise*

The first model proposed by Strintzis, Kokkinidis [22] is to use multiplicative Rayleigh distributed noise to represent speckle patterns. The imaging process is described by

$$u(x) = v(T(x)) \cdot \varepsilon \quad (15)$$

with the Rayleigh distribution

$$P(y) = \frac{\pi \cdot y}{2} \cdot \exp\left(-\frac{\pi \cdot y^2}{4}\right), \quad y > 0 \quad (16)$$

having the variance  $\frac{2}{\pi}$ . Setting it into the MLE framework, equation (4), leads to:

$$\log \mathcal{L}(T, \varepsilon) = \log \prod_{x_k \in \Omega} \frac{1}{v(T(x_k))} P\left(\frac{u(x_k)}{v(T(x_k))}\right) \quad (17)$$

$$\approx \sum_{x_k \in \Omega} \log\left(\frac{u(x_k)}{v(T(x_k))^2}\right) - \frac{\pi}{4} \frac{u(x_k)^2}{v(T(x_k))^2}. \quad (18)$$

*SK<sub>2</sub>: Signal dependent Gaussian noise*

The second model proposed by Strintzis and Kokkinidis [22] uses signal dependent additive Gaussian distributed noise, being expressed by

$$u(x) = v(T(x)) + \sqrt{v(T(x))} \cdot \varepsilon. \quad (19)$$

Setting it once again into the MLE framework leads to:

$$\log \mathcal{L}(T, \varepsilon) = \log \prod_{x_k \in \Omega} \frac{1}{\sqrt{v(T(x_k))}} \exp\left(-\frac{[u(x_k) - v(T(x_k))]^2}{2 \cdot \sigma^2 \cdot v(T(x_k))}\right) \quad (20)$$

$$= \sum_{x_k \in \Omega} -\log[v(T(x_k))] - \frac{[u(x_k) - v(T(x_k))]^2}{2 \cdot \sigma^2 \cdot v(T(x_k))}. \quad (21)$$

*CD<sub>1</sub>: Division of Rayleigh noises*

The noise models of Strintzis, Kokkinidis [22] consider only one image to be degraded by noise, the other one has to be noiseless, which is not possible in practice. Cohen, Dinstein [23] assume each image to be contaminated by multiplicative Rayleigh noises  $\varepsilon_1$  and  $\varepsilon_2$ , respectively. This leads to the following noise model

$$u(x) = v(T(x)) \cdot \varepsilon \quad \text{with} \quad \varepsilon = \frac{\varepsilon_1}{\varepsilon_2} \quad (22)$$

and the probability density function for a division of Rayleigh noises is:

SK <sub>1</sub>	SK <sub>2</sub>
$\sum_{i \neq j} \omega_{i,j} \cdot \mathbb{E} \left[ \log \left( \frac{u_i}{u_j^2} \right) - \frac{\pi}{4} \frac{u_i^2}{u_j^2} \right]$	$\sum_{i \neq j} \omega_{i,j} \cdot \mathbb{E} \left[ \log u_j + \frac{(u_i - u_j)^2}{u_j} \right]$
CD <sub>1</sub>	CD <sub>2</sub>
$\sum_{i \neq j} \omega_{i,j} \cdot \mathbb{E} \left[ \log \frac{u_i}{u_j} \left( \left( \frac{u_i}{u_j} \right)^2 + 1 \right)^{-2} \right]$	$\sum_{i \neq j} \omega_{i,j} \cdot \mathbb{E} [\tilde{u}_i - \tilde{u}_j - \log(e^{2(\tilde{u}_i - \tilde{u}_j)} + 1)]$

Table 4

Summary of multivariate ultrasound specific similarity measures.

$$P(y) = \frac{2 \cdot y}{(y^2 + 1)^2}, y > 0. \quad (23)$$

The probability density function results from the division of two Rayleigh distributed random variables [26]. The log-likelihood function is:

$$\log \mathcal{L}(T, \varepsilon) = \log \prod_{x_k \in \Omega} \frac{1}{v(T(x_k))} P \left( \frac{u(x_k)}{v(T(x_k))} \right) \quad (24)$$

$$= \log \prod_{x_k \in \Omega} \frac{1}{v(T(x_k))} \frac{2 \cdot \frac{u(x_k)}{v(T(x_k))}}{\left( \left( \frac{u(x_k)}{v(T(x_k))} \right)^2 + 1 \right)^2} \quad (25)$$

$$= \sum_{x_k \in \Omega} \log \frac{2 \cdot u(x_k)}{v(T(x_k))^2} - 2 \cdot \log \left[ \left( \frac{u(x_k)}{v(T(x_k))} \right)^2 + 1 \right] \quad (26)$$

$$\approx \sum_{x_k \in \Omega} \log u(x_k) - \log v(T(x_k)) - \log \left[ \left( \frac{u(x_k)}{v(T(x_k))} \right)^2 + 1 \right]. \quad (27)$$

*CD<sub>2</sub>: Logarithm of division of Rayleigh noises*

The second model by Cohen, Dinstein [23] considers next to the noise contamination of both images also the log-compressed nature of ultrasound images by applying the logarithm to equation (22), leading to:

$$\log u(x) = \log[v(T(x)) \cdot \varepsilon] \quad (28)$$

$$= \log v(T(x)) + \log \varepsilon. \quad (29)$$

With setting  $\tilde{u}(x) = \log u(x)$  and  $\tilde{v}(x) = \log v(T(x))$

$$\varepsilon(x) = \exp(\tilde{u}(x) + \tilde{v}(x)) \quad (30)$$

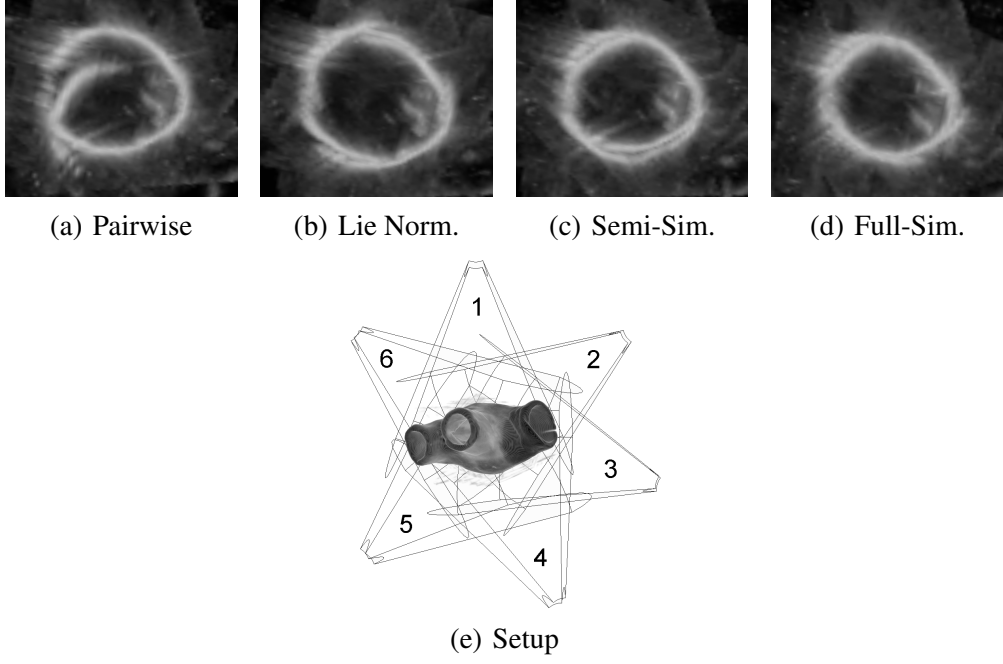


Fig. 3. Error accumulation with pairwise registration. Simultaneous registration intrinsically deals with it.

leading to the log-likelihood function:

$$\log \mathcal{L}(T, \varepsilon) = \log \prod_{x_k \in \Omega} \frac{\exp(\tilde{u}(x_k))}{\exp(\tilde{v}(x_k))} \cdot P(\exp(\tilde{u}(x_k) - \tilde{v}(x_k))) \quad (31)$$

$$= \log \prod_{x_k \in \Omega} \frac{\exp(\tilde{u}(x_k))}{\exp(\tilde{v}(x_k))} \cdot \frac{2 \cdot \exp(\tilde{u}(x_k) - \tilde{v}(x_k))}{[\exp(\tilde{u}(x_k) - \tilde{v}(x_k))^2 + 1]^2} \quad (32)$$

$$= \log \prod_{x_k \in \Omega} \frac{2 \cdot \exp(2(\tilde{u}(x_k) - \tilde{v}(x_k)))}{[\exp(2(\tilde{u}(x_k) - \tilde{v}(x_k))) + 1]^2} \quad (33)$$

$$\approx \sum_{x_k \in \Omega} \tilde{u}(x_k) - \tilde{v}(x_k) - \log[\exp(2(\tilde{u}(x_k) - \tilde{v}(x_k))) + 1]. \quad (34)$$

#### 4.1 Multivariate Extension

Essential for the usage of simultaneous registration strategies are multivariate similarity measures. We directly set the presented, ultrasound specific likelihood terms in the extension shown in equation (7), which accumulates the bivariate terms. A summary of the multivariate extensions of the similarity measures is shown in Table 4. To make the table clearer we set  $u_i = u_i(T_i(\cdot))$ ,  $u_j = u_j(T_j(\cdot))$ ,  $\tilde{u}_i = \log u_i(T_i(\cdot))$ , and  $\tilde{u}_j = \log u_j(T_j(\cdot))$ . The weighting factors  $\omega_{i,j}$  emphasize image pairs with high overlap.

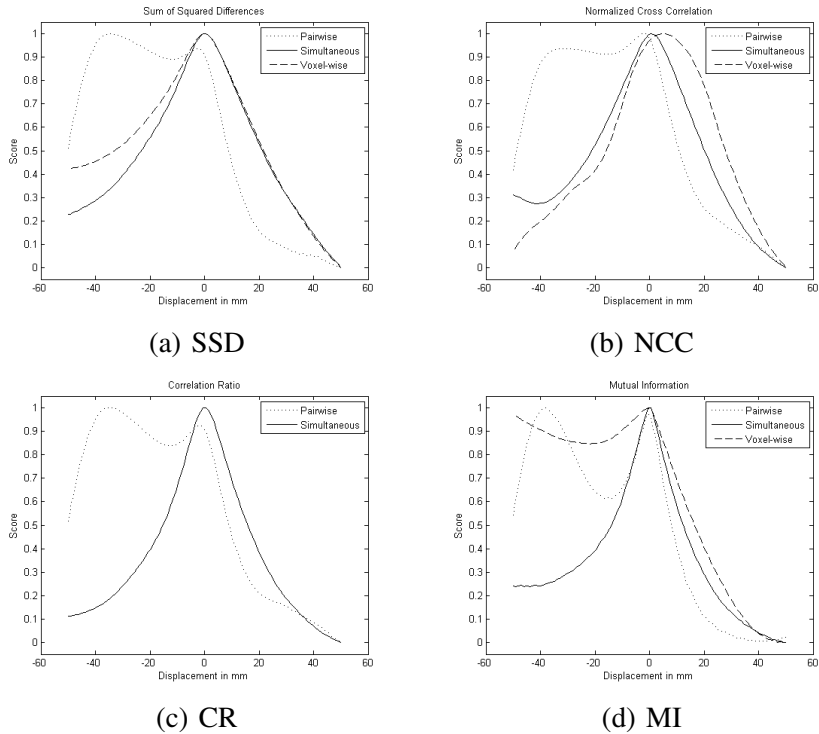


Fig. 4. Similarity plots of the measures in Table 3 on the baby phantom. The bivariate measures are shown by a dotted line, the multivariate ones by a solid line, and the voxel-wise ones by a dashed line (x-axis: displacement in mm, y-axis: score).

## 5 Results

We tested the mosaicing strategies and multivariate similarity measures on images from a heart clay model and from a baby phantom. During our experiments we tried several non-linear optimization methods such as Hill-Climbing, Powell-Brent, and Downhill-Simplex [27], where we obtained the best results with the Downhill-Simplex optimizer.

For the first experiment, 3D images of a heart clay model in the water bath were acquired from six different angles. The imaging setup is shown in Figure 3(e). We use a cutting plane through the reconstruction volume to visualize the registration error. The registrations are performed using SSD. When using pairwise registration the summed up error leads to a large displacement between the first and sixth volume, Figure 3(a). The pairwise registration with a successive Lie normalization corrects this error, but the alignment is not perfect, Figure 3(b). The semi-simultaneous registration provides good results, Figure 3(c), but superior results are obtained with the full-simultaneous registration, Figure 3(d).

The second data set consists of four sequentially taken acquisitions from a baby phantom, see Figure 1 for the compounded result. We use it to evaluate the presented bi- and multivariate similarity measures. Each acquisition has a resolution

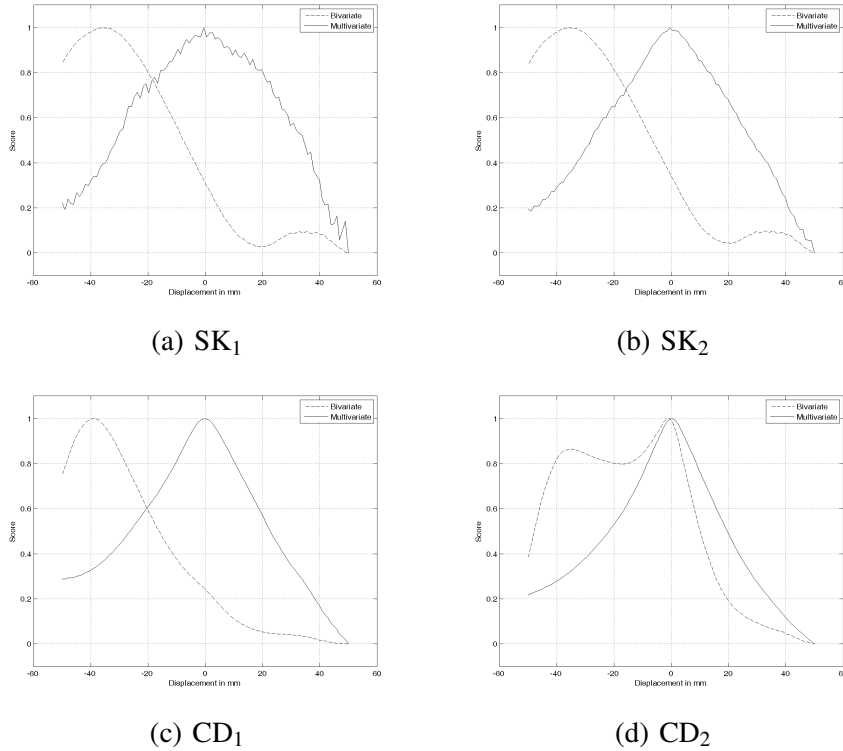


Fig. 5. Similarity plots of the measures in Table 4 on the baby phantom. The bivariate measures are shown by a dashed line, the multivariate ones by a solid line (x-axis: displacement in mm, y-axis: score).

of  $64 \times 64 \times 64$  voxels. We plot the similarity measures by moving the second volume along the cranio-caudal axis and evaluate the associated score values, see Figures 4 and 5. More precisely, for bivariate similarity measures the similarity of the second volume with respect to the third one is measured, for multivariate measures the similarity of the second volume with respect to the other three volumes is measured. The correct alignment of the volumes is at a displacement of 0.0 mm, and the total overlap of the neighboring volumes is at -37.0 mm displacement.

Analyzing first the standard similarity measures, see Figure 4, one clearly recognizes the high overlap dependence of the bivariate measures, being a source for misregistrations. All measures except NCC only have local optimum at the correct alignment of the volumes, but a global optimum at the point of total overlap. And also for NCC the optimum is not very distinctive. In contrast, the multivariate measures provide a smooth cost function with a clear maximum at the correct position.

Taking a look at the ultrasound specific measures, the bivariate versions of  $SK_1$ ,  $SK_2$ , and  $CD_1$  also favor the total overlap, see Figures 5(a) - 5(c). The situation changes for  $CD_2$ , where we have in fact a nice optimum at the correct alignment, see Figure 5(d). In the multivariate case, all measures show a clear optimum for the correct alignment, but the curves for  $CD_1$  and  $CD_2$  are smoother and more distinctive. These results are corresponding to those of Cohen, Dinstein [23] and

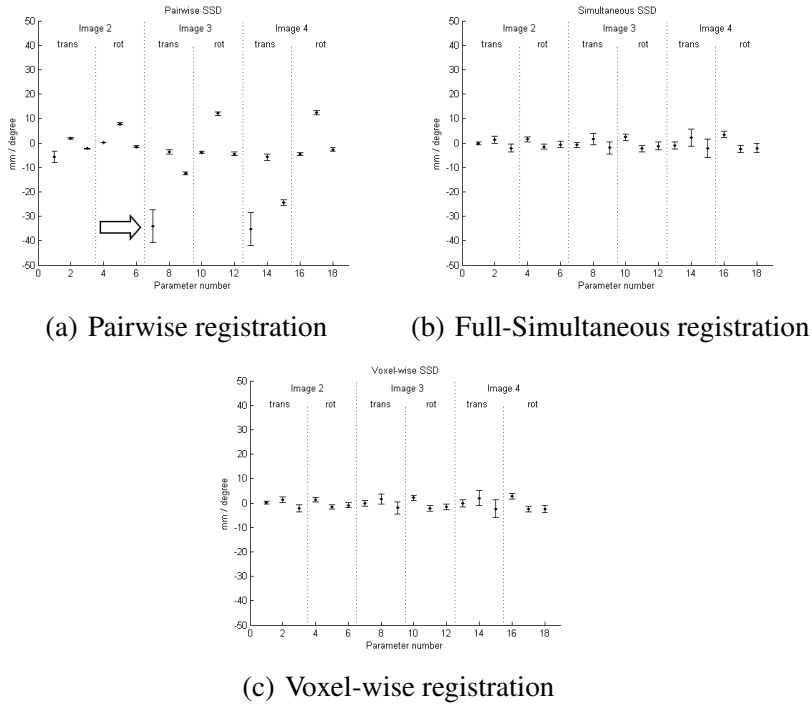


Fig. 6. Mean and standard deviation of pose parameters after 100 registrations.

Boukerroui *et al.* [24].

We also ran a registration study on the phantom baby, with an initial random deviation of maximal  $\pm 20$  mm in translation and  $\pm 20^\circ$  in rotation from the correct pose. The mean and standard deviation of each pose parameter of the three moving images after the registration are shown in Figure 6. The pairwise registration leads to a misalignment because of the total overlap of the images 2 and 3, indicated in Figure 6(a) by a mean of -34.9 mm of parameter 7. The distribution of the mean values around 0 after the simultaneous registration, together with low variances, indicates good registration results, see Figure 6(b) and 6(c).

## 6 Conclusion

We have described three registration strategies for ultrasound mosaicing which are put into relationship to the standard pairwise sequential one. Our experiments clearly show that these advanced strategies are necessary to address the problems that can occur during ultrasound mosaicing. The best registration result was obtained with the full-simultaneous approach but this comes with a high computational cost. Moreover, we set up a MLE framework to deduce extensions of popular similarity measures. This allows us to derive a new class of multivariate measures by summing up the pairwise ones and also to deduce a voxel-wise extension of SSD.

Additionally, we adapted the registration framework to the peculiarities of ultrasound registration, by using various noise models, which seem to be better suited than the standard additive Gaussian noise. This enables the derivation of ultrasound specific similarity measures. The multivariate versions of these measures are obtained by using the afore mentioned multivariate extension of the MLE framework.

Our experiments show, that bivariate similarity measures have problems with the partial overlap, clearly favoring a total overlap of the volumes.  $CD_2$  performs best by correctly indicating the spatial alignment of the volumes. This may be attributed to the considered log-compression of the US images and the better adapted noise model, which considers both images to be degraded by a Rayleigh distributed noise. In the case of multivariate similarity measures the general performance was much better. Further experiments will have to be conducted to better differentiate the multivariate similarity measures, but the results from the bivariate ones already indicated the necessity for ultrasound specific measures.

In the future, we would like to investigate the usage of non-rigid registration approaches within our ultrasound mosaicing framework. This helps to address problems coming from deformations during the image acquisition *e.g.* the movement of a baby. Also part of future research will be the actual spatial compounding of the registered volumes, where Soler *et al.* [28] presented a nice overview, and for which Wachinger *et al.* [29] recently proposed a novel approach, based on the estimation of the acoustic impedance.

## List of Figures

1	Volume rendering of compounded baby phantom.	4
2	Registration graphs illustrating different strategies. Solid lines indicating calculated transformations and dashed lines deduced ones. For clarity, not all edges are labeled.	5
3	Error accumulation with pairwise registration. Simultaneous registration intrinsically deals with it.	13
4	Similarity plots of the measures in Table 3 on the baby phantom. The bivariate measures are shown by a dotted line, the multivariate ones by a solid line, and the voxel-wise ones by a dashed line (x-axis: displacement in mm, y-axis: score).	14
5	Similarity plots of the measures in Table 4 on the baby phantom. The bivariate measures are shown by a dashed line, the multivariate ones by a solid line (x-axis: displacement in mm, y-axis: score).	15
6	Mean and standard deviation of pose parameters after 100 registrations.	16

## List of Tables

1	Algorithm for pairwise registration with Lie group normalization.	6
2	Algorithm for semi-simultaneous registration.	7
3	Summary of bi- and multivariate similarity measures in shortened notation.	9
4	Summary of multivariate ultrasound specific similarity measures.	12

## References

- [1] Z. Wang, G. Slabaugh, G. Unal, T. Fang, Registration of ultrasound images using an information-theoretic feature detector, *Biomedical Imaging: From Nano to Macro*, 2007. ISBI 2007. 4th IEEE International Symposium on (2007) 736–739.
- [2] S. H. Kim, B. I. Choi, K. W. Kim, K. H. Lee, J. K. Han, Extended Field-of-View Sonography: Advantages in Abdominal Applications, *Journal of Ultrasound in Medicine* 22 (4) (2003) 385–394.
- [3] P. Peetrons, Ultrasound of muscles, *European Radiology* 12 (1) (2002) 35–43.
- [4] Y. Leung, A. Roshier, S. Johnson, R. Kerslake, D. McNally, Demonstration of the appearance of the paraspinal musculoligamentous structures of the cervical spine using ultrasound., *Clin Anat* 18 (2) (2005) 96–103.
- [5] M. Ying, M.-H. Sin, Comparison of extended field of view and dual image ultrasound techniques: Accuracy and reliability of distance measurements in phantom study, *Ultrasound in Medicine & Biology* 31 (2005) 79–83.
- [6] C. Dietrich, A. Ignee, M. Gebel, B. Braden, G. Schuessler, Imaging of the abdomen, *Z Gastroenterol* 40 (2002) 965–970.
- [7] W. Henrich, A. Schmider, S. Kjos, B. Tutschek, J. W. Dudenhausen, Advantages of and applications for extended field-of-view ultrasound in obstetrics, *Archives of Gynecology and Obstetrics* V268 (2003) 121–127.
- [8] H. Kuhl, M. Schreckenber, D. Rulands, M. Katoh, W. Schafer, G. Schummers, A. Bucker, P. Hanrath, A. Franke, High-resolution transthoracic real-time three-dimensional echocardiography Quantitation of cardiac volumes and function using semi-automatic border detection and comparison with cardiac magnetic resonance imaging, *Journal of the American College of Cardiology* 43 (11) (2004) 2083–2090.
- [9] C. Jenkins, K. Bricknell, L. Hanekom, T. Marwick, Reproducibility and accuracy of echocardiographic measurements of left ventricular parameters using real-time three-dimensional echocardiography, *Journal of the American College of Cardiology* 44 (4) (2004) 878–886.
- [10] A. H. Gee, G. M. Treece, R. W. Prager, C. J. C. Cash, L. H. Berman, Rapid registration for wide field-of-view freehand 3d ultrasound., *IEEE Trans. Med. Imaging* 22 (11) (2003) 1344–1357.
- [11] T. Poon, R. Rohling, Three-dimensional extended field-of-view ultrasound, *Ultrasound in Medicine and Biology* 32 (3) (2005) 357–369.
- [12] M. ODonnell, R. Skovoroda, Internal Displacement and Strain Imaging Using Ultrasonic Speckle Tracking, *IEEE Trans. on Ultrasonics, Ferroelectrics, and Frequency Control* (1994) 41 (3).
- [13] G. P. Penney, J. M. Blackall, M. S. Hamady, T. Sabharwal, A. Adam, D. J. Hawkes, Registration of freehand 3d ultrasound and magnetic resonance liver images, *Medical Image Analysis* 8 (1) (2004) 81–91.

- [14] K. Abd-Elmoniem, A. Youssef, Y. Kadah, Real-time speckle reduction and coherence enhancement in ultrasound imaging via nonlinear anisotropic diffusion, *Biomedical Engineering, IEEE Transactions on* 49 (9) (2002) 997–1014.
- [15] C. Kotropoulos, X. Magnisalis, I. Pitas, M. Strintzis, Nonlinear ultrasonic image processing based on signal-adaptive filters and self-organizing neural networks, *Image Processing, IEEE Transactions on* 3 (1) (1994) 65–77.
- [16] X. Pennec, Statistical computing on manifolds for computational anatomy, *Habilitation à diriger des recherches, Université Nice Sophia-Antipolis* (Dec. 2006).
- [17] T. Vercauteren, A. Perchant, G. Malandain, X. Pennec, N. Ayache, Robust mosaicing with correction of motion distortions and tissue deformation for in vivo fibered microscopy, *Medical Image Analysis* 10 (5) (2006) 673–692.
- [18] L. Zollei, E. Learned-Miller, E. Grimson, W. W. III, Efficient population registration of 3d data, in: *ICCV, 2005*, pp. 291–301.
- [19] R. Benjemaa, F. Schmitt, Fast global registration of 3D sampled surfaces using a multi-z-buffer technique, *Image and Vision Computing* 17 (2) (1999) 113–123.
- [20] P. A. Viola, Alignment by maximization of mutual information, Ph.d. thesis, Massachusetts Institute of Technology (1995).
- [21] A. Roche, G. Malandain, N. Ayache, Unifying maximum likelihood approaches in medical image registration, *International Journal of Imaging Systems and Technology: Special Issue on 3D Imaging* 11 (1) (2000) 71–80.
- [22] M. Strintzis, I. Kokkinidis, Maximum likelihood motion estimation in ultrasound image sequences, *Signal Processing Letters, IEEE* 4 (6) (1997) 156–157.
- [23] B. Cohen, I. Dinstein, New maximum likelihood motion estimation schemes for noisy ultrasound images, *Pattern Recognition* 35 (2) (2002) 455–463.
- [24] D. Boukerroui, J. Noble, M. Brady, Velocity estimation in ultrasound images: a block matching approach., *Inf Process Med Imaging* 18 (2003) 586–98.
- [25] J. Revell, M. Mirmehdi, D. McNally, Combined ultrasound speckle pattern similarity measures, in: *Medical Image Understanding and Analysis, BMVA Press, 2004*, pp. 149–153.
- [26] A. Papoulis, U. S. Pillai, *Probability, Random Variables and Stochastic Processes*, McGraw-Hill, 2001.
- [27] W. Press, S. Teukolsky, W. Vetterling, B. Flannery, *Numerical recipes in C: the art of scientific computing*, Cambridge University Press, 2002.
- [28] P. Soler, G. Delso, N. Villain, E. Angelini, I. Bloch, Superresolution spatial compounding techniques with application to 3D breast ultrasound imaging, in: *SPIE Medical Imaging 2006: Ultrasonic Imaging and Signal Processing.*, Vol. 6147, 2006, pp. 281–292.
- [29] C. Wachinger, R. Shams, N. Navab, Estimation of acoustic impedance from multiple ultrasound images with application to spatial compounding, *IEEE Computer Society Workshop on Mathematical Methods in Biomedical Image Analysis (MMBIA 2008)*.